PAPER • OPEN ACCESS

Growth dynamics of nanocolumnar thin films deposited by magnetron sputtering at oblique angles

View the article online for updates and enhancements.

Growth dynamics of nanocolumnar thin films deposited by magnetron sputtering at oblique angles

R Alvarez[1,2,*] , A Garcia-Valenzuela[1] , G Regodon[1], F J Ferrer[3],
V Rico[1] , J M Garcia-Martin[4] , A R Gonzalez-Elipe[1] and A Palmero[1,*]

[1] Instituto de Ciencia de Materiales de Sevilla (CSIC-US), Américo Vespucio 49, E-41092 Seville, Spain
[2] Departamento de Física Aplicada I. Escuela Politécnica Superior, Universidad de Sevilla, Virgen de África 7, E-41011 Seville, Spain
[3] Centro Nacional de Aceleradores (CSIC-US), Thomas A. Edison 7, E-41092, Seville, Spain
[4] Instituto de Micro y Nanotecnología, IMN-CNM, CSIC (CEI UAM+CSIC), Isaac Newton 8, E-28760 Tres Cantos, Spain

E-mail: ralvarezmol@us.es and alberto.palmero@csic.es

CrossMark

Abstract

The morphology of numerous nanocolumnar thin films deposited by the magnetron sputtering technique at oblique geometries and at relatively low temperatures has been analyzed for materials as different as Au, Pt, Ti, Cr, TiO_2, Al, HfN, Mo, V, WO_3 and W. Despite similar deposition conditions, two characteristic nanostructures have been identified depending on the material: a first one defined by highly tilted and symmetric nanocolumnar structures with a relatively high film density, and a second one characterized by rather vertical and asymmetric nanocolumns, with a much lower film density. With the help of a model, the two characteristic nanostructures have been linked to different growth dynamics and, specifically, to different surface relaxation mechanisms upon the incorporation of gaseous species with kinetic energies above the surface binding energy. Moreover, in the case of Ti, a smooth structural transition between the two types of growths has been found when varying the value of the power used to maintain the plasma discharge. Based on these results, the existence of different surface relaxation mechanisms is proposed, which quantitatively explains numerous experimental results under the same conceptual framework.

Supplementary material for this article is available online

Keywords: magnetron sputtering, oblique angle deposition, nanocolumns, hyperthermal processes

1. Introduction

Porous thin films produced by physical vapor deposition (PVD) techniques at oblique angles have been extensively studied in the last years due to their singular structural features and properties [1]. These films are formed by well-separated tilted columnar structures with diameters of a few tens of nanometers that provide singular morphological features, e.g. large specific surfaces, high surface roughness, open/embedded porosity, etc [2, 3]. Thanks to these features, nanocolumnar thin films have found applications in numerous fields, such as microfluidics, plasmonics, sensors, medicine, solar cells, aerospace industry or hydrogen storage, among others [4–14]. Moreover, they are also useful to perform fundamental studies, as any relevant atomistic mechanism

during growth may leave specific traces on the morphology of the nanocolumns (e.g. affecting the tilt angle, columnar shape, preferential coalescence, typical separation distance, etc) [1]. In general terms, the nanocolumnar growth emerges thanks to a particular experimental arrangement, the so-called oblique angle configuration, by which vapor deposition species are made to arrive at the substrate along a preferential oblique direction, inducing surface shadowing mechanisms. These processes are responsible for the appearance of shadowed regions on the film surface, i.e. regions behind each mound where the deposition is inhibited and that eventually become large intercolumnar pores upon growth [1].

Classically, nanocolumnar films were grown by the evaporation technique at glancing angles, in which the deposition species stems from a sublimated solid source in a vacuum reactor [15]. Last decade, however, has witnessed the development of more versatile and industrially scalable methodologies, such as the magnetron sputtering technique at oblique angles (MS-OAD), by which the interaction between a plasma and a solid target causes the sputtering of species from the latter, preferentially in the direction perpendicular to its surface, that are subsequently deposited on a substrate [16, 17]. In this case, the two key conditions to operate at oblique angles are: (i) the sputtered species must arrive at the substrate following a common preferential direction of movement, and (ii) the arrangement in the deposition reactor must allow the oblique angle incidence of sputtered species on the substrate. The first one is usually achieved by working at relatively low pressures, in a typical ballistic transport regime, thus minimizing the number of elastic scatterings of sputtered particles on plasma heavy species [1]. The second condition, on the other hand, is usually achieved by tilting the substrate with respect to the target, although other alternatives have been presented in the literature [18, 19]. Interestingly, and despite the similarities between films grown by evaporation and MS-OAD under equivalent geometrical conditions, the atomistic phenomena in either case is known to be very different: while deposition species in the gas phase possess typical kinetic energies below 0.1 eV in evaporation, in MS-OAD they may reach few tens eV, above the binding energy of surface atoms in the film [16, 17]. This means that, unlike in evaporation, hyperthermal (HT) mechanisms can be triggered in MS-OAD, i.e. mobility processes of film surface atoms induced by the incorporation of film forming species with relatively high kinetic energy [20–22]. In addition to these processes, key quantities regarding the film growth and nanostructural development are the so-called normalized energy and momentum fluxes, also known as energy per atom (EPA) or momentum per atom (MPA) [23]. They are defined as the total energy or momentum flux deposited in the film, no matter the particular source or transfer mechanism (absorption of photons, ion impingement [24], impingement of fast neutrals, etc), divided by the flux of deposition atoms. Using these quantities, many different energy-related and momentum-related phenomena in classical non-oblique growth conditions have been explained: while the EPA has been linked to microstructural changes in the film, the MPA has been associated to changes in film density and stress [25, 26].

For instance, Abadias *et al* [27] found a straightforward connection between these fluxes and the type of stress in TiN thin films, from tensile to compressive values, while Xia *et al* demonstrated that these fluxes defined the texture of Y_2O_3 thin films, finding a smooth shift in the crystalline texture from a monoclinic B phase (1 1 1) orientation to a minority cubic C phase, as well as a shift in film density and residual stress [26]. Furthermore, Konstantinidis *et al* found that the phase constitution of TiO_2 is intimately correlated to the value of these fluxes [28]. Indeed, there are numerous examples in the literature that indicate that the energy and momentum fluxes towards the film in magnetron sputtering depositions affect the dynamic state of surface atoms and the growth process [23], although the affected atomistic mechanisms are yet to be identified and understood [28], a fact that has discouraged their inclusion in growth simulation models.

The intrinsic connection between HT processes and the tilt angle of the nanocolumns in MS-OAD was demonstrated in [29]. There, we showed that Ti thin films deposited by evaporation and MS-OAD under equivalent geometrical conditions were formed by nanocolumns with very different morphologies: while those in the evaporated film were thin and highly tilted, those produced by MS-OAD were thick and almost vertical. This difference was explained by means of a well-tested growth model, thanks to which it was demonstrated that HT processes were responsible for triggering numerous displacements of surface atoms in the direction of the arriving particles, thus straightening the columns up [30]. The inclusion of HT processes in the model did not only quantitatively reproduce the tilt angle of the columnar structures by MS-OAD but also their shape and film density under numerous experimental conditions [30]. Moreover, the solutions of the same model in absence of HT processes reproduced quite well the morphological features and density of evaporated Ti thin films, a result that is congruent with the low energy of the deposition species and the inhibition of HT processes when employing this technique [29].

Even though the influence of HT processes in MS-OAD was demonstrated in [30], there are still many issues unsolved that require further research and explanation. For instance, in [29] it was found that the sole increase of the power employed to maintain the sputter plasma during the deposition of Ti caused the progressive tilt of the nanocolumns from almost vertical to angles very similar to those obtained by evaporation. This agrees with some studies in the literature that report nanocolumnar structures deposited by MS-OAD as tilted as those grown by evaporation [31–33], a remarkable result that demands a thorough explanation. Based on all the ideas above, in this paper the growth and nanostructure of numerous materials deposited by MS-OAD are analyzed: for a primary assessment, the growth of Au, Pt, Ti and W is studied in detail and, subsequently, a broad set of data taken from the literature on Ti, TiO_2, Cr, Al, HfN, Mo, V, WO_3 and W. As a result, it is demonstrated the existence of two different growth modes that lead to two different characteristic nanostructures, despite the similar deposition conditions. While some films are rather dense and defined by highly tilted and symmetric nanocolumnar structures, some others possess much lower

densities and depict rather vertical and asymmetric nano-columns. With the help of a model, these two growth modes are linked to different surface relaxation schemes upon the arrival of deposition species with relatively high kinetic energy during growth. Moreover, and under the light of the obtained results, in the final part of the paper the morphological transition of the Ti nanocolumns with power reported in [29] is analyzed, and the origin of the two relaxation schemes is discussed.

2. Experimental

The experimental data have been explicitly obtained for this paper or taken from the literature for films deposited by DC MS-OAD at (i) relatively low pressures, and (ii) low substrate temperatures. The first condition was imposed to make the mean free path of sputtered species in the plasma as long as possible and minimize collisions with plasma heavy species, responsible not only for their scattering and loss of a preferential direction of movement, but also for reducing their kinetic energy and thus the influence of HT processes. The second condition was imposed to minimize the influence of any thermally-induced mobility process in the film that may overlap with the HT mechanism [34, 35]. Consequently, the deposition conditions have been chosen to enhance the role of HT processes in the film growth and to minimize the influence of any other potentially competing mechanism that could produce atomic mobility.

Four different materials have been analyzed in detail in terms of columnar morphology, tilt angle (β) and density (ρ): Ti, Au, Pt and W, deposited under different configurations and in different reactors to avoid any system-biased results (see table 1). The depositions of Pt and W thin films were specifically carried out for this work: a cylindrical vacuum reactor was employed, equipped with 1 and 3 inch diameter sputtering targets of Pt and W respectively. The plasma gas in both cases was Ar (purity 99.995%) and the working pressure was set to the minimum value at which the plasmas was stable: 0.4 Pa in the case of Pt depositions, and 0.2 Pa in the case of W. The substrate holder was placed at 7 cm from the target and rotated an angle α of $0°$, $50°$, $65°$, $75°$, $85°$ and $90°$ in the case of Pt, and $0°$, $45°$, $70°$, $80°$, $85°$, $90°$ and $100°$ in the case of W. Please note that α refers to the rotation angle of the substrate, which can be different form the angle of incidence of the sputtered species. In general terms, these species arrive at the substrate following an incident angle distribution function due to the non-punctual shape of the racetrack and to their different collisional transport in the plasma gas, which depends on quantities such as the gas pressure, the shape of the target, the target-substrate distance, etc. A relevant quantity when operating in typical OAD conditions is the angle aligning the racetrack and the substrate, α_b. This angle defines the angle of arrival of sputtered species that have experienced no elastic scatterings with plasma species and, hence, it provides information on the angle of arrival of ballistic species. In the case of circular targets, and when the substrate is placed along the central axis of the target, α and

α_b are related by $\alpha_b = \alpha - \Delta$, with $\Delta = \arctan(R/L)$, L being the target-substrate distance and R the radius of the racetrack [18]. In the case of Pt, it amounts to $\Delta \sim 5°$, while in the case of W to $\Delta \sim 15°$. Preparations were carried out using a DC power supply at a constant value of 40 W (Pt) and 300 W (W). The deposition time was taken to obtain films with thicknesses of ~ 300 nm (Pt) and ~ 1000 nm (W). The morphology of the Pt and W nanocolumns was analyzed by means of field emission scanning electron microscopy (FESEM). In addition, Rutherford backscattering spectroscopy (RBS) was employed to assess their atomic areal density: experiments were carried out in the 3 MV tandem accelerator of the National Center for Accelerators (Seville, Spain) with a beam of 1.5 MeV alpha particles and a passivated implanted planar silicon (PIPS) detector located at $165°$ scattering angle, with accumulated doses about 1.5 μC, and ~ 1 mm beam spot diameter. The RBS spectra were simulated with the SIMNRA code [36], whereas ρ was calculated by dividing the areal density by the film thickness, as obtained from the cross-sectional FESEM image at a location next to the RBS beam spot. The uncertainty of ρ has been estimated to be between 5% and 10% of its numerical value, given the uncertainties of the RBS measurement and of the thickness determination of columnar films with high surface roughness.

The data from the Au thin films were taken from [37] (see table 1 for deposition conditions). As mentioned above, only the set grown at the lowest pressure value in that paper (0.15 Pa) was chosen, with α set to $0°$, $45°$, $60°$, $70°$, $80°$, $85°$ and $87.5°$, with a negligible value of Δ. Moreover, in [37] the focus was on the tilt angle of the nanocolumns as a function of the deposition conditions. That is why, in this paper, the density of these layers was explicitly measured following the same procedure as for the Pt and W films described above.

The data regarding the Ti thin films considered in this paper were taken from different sources (see table 1):

(i) Reference [30], where the films were deposited far from the plasma, and where the nanostructure and density of the films were presented. Following the same approach as before, the low-pressure cases (0.15 Pa) were analyzed for α set to $0°$, $45°$, $60°$, $70°$, $80°$ and $85°$, with a negligible value of Δ. Although the columnar structures were rather vertical, the tilt angle of the columns with respect to the substrate normal, β, was not specifically measured in [30]. Therefore, for this work, this angle has been measured using the FESEM images. Also, in [30] a full analysis on the crystalline features of these films is performed.

(ii) The films studied in [29], where the deposition was carried out using collimators to maximize the deposition of ballistic high energy atoms, keeping the same geometrical conditions ($\alpha = 95°$, with $\Delta \sim 15°$) while increasing the power supplied to maintain the plasma. There, a complete analysis on the film nanostructures and densities were carried out.

(iii) For comparison purposes, Ti thin films were also grown by evaporation at glancing angles on Si substrates, with α set to $0°$, $65°$, $70°$, $80°$ and $85°$ in an experimental setup

4

Table 1. List of experimental conditions employed to deposit the films and analyze both, tilt angle, β, and density, ρ, of the nanocolumnar structures, together with the references from which the values were taken. The experimental data required to solve the model are also included in the framed region. The symbol ϕ denotes the target radius. The data containing (*) have been estimated (the gas temperature was set to 350 K in all the cases, while the racetrack was placed at a position half the radius of the target).

Film	p_g (Pa)	Target-Film distance (cm)	Target diameter (inches)	Target potential (V)	Substrate rotation angle (°)	DC Power (W)	β (°)	ρ (%)
Evaporated Ti	10^{-4}	50	—	—	0–85	—	This Work	This Work
Au	0.15 (Ar)	19	$\phi = 1.5$	150	0–87.5	100	[37]	This work
Ti	0.15 (Ar)	22	$\phi = 2$	150	0–85	300	This Work	[30]
W	0.2 (Ar)	7	$\phi = 3$	300	0–100	300	This Work	This Work
Pt	0.4 (Ar)	7	$\phi = 1$	100	0–90	40	This Work	This Work
TiO$_2$	0.2 (Ar), 0.05(O$_2$)	7	$\phi = 3$	300	60–85	300	[38]	[38]
Cr	0.53 (Ar)	8.5	$\phi = 2$	300*	0–80	N.A.	[39]	[39]
Ti	0.15 (Ar)	7	$\phi = 3$	300	95	25–400	[29]	[29]

already described in [15]. These films were characterized by FESEM as well as by RBS to obtain the tilt angle of the nanocolumns and their density as a function of α (in this case, α refers to the angle aligning the evaporation source and the substrate with respect to the substrate normal).

In addition to these 4 materials, data from the literature on Cr and TiO$_2$ (see table 1) were taken to complete the discussion. Results on TiO$_2$ thin films grown by MS-OAD were taken from [38], where both film density and tilt angle of the nanocolumns were measured as a function of α (values set at 60°, 70°, 80° and 85°) following the same procedure described above. Moreover, data on Cr thin films for α set to 0°, 30°, 60° and 80° were taken from [39], where β was obtained from the SEM images and ρ by means of x-ray reflectivity measurements at grazing incidence. Since no uncertainty is mentioned in that reference for ρ, 10% error bars have been included here. Finally, the growth of different materials by MS-OAD has been analyzed, such as Al, Cr and Ti [32], HfN [40], Ti and Mo [41], Ti [31], V [42, 43], WO$_3$ [44], and W [45, 46].

3. Growth model and surface relaxation schemes

3.1. Growth model

The growth model, which was presented in [30], does not consider any thermally-induced mechanisms, and has already been tested under numerous low temperature growth situations. However, some modifications have been introduced regarding the surface relaxation schemes, which will be explained and discussed below. For the sake of clarity, next we describe its fundamentals (please, check figure 1 for a scheme of the model).

In a first stage, the model makes use of the SRIM code [47], which provides the momentum distribution of sputtered species from the target due to the plasma ion impingement, $F(\vec{p})$, given the target material, the ion chemical nature (which is argon in all the presented cases) and the ion energy, estimated as eV_0, with e the charge of the electron and V_0 the target voltage. Effectively, the SRIM output is a list of different sputtered particles that includes the ejection direction and kinetic energy, from which the corresponding distributions functions can be obtained. However, given the important correlation existing between these two magnitudes, it is more adequate to describe the ejection of sputtered particles by means of a momentum vector distribution. The SRIM output is then introduced into the SIMTRA code [48, 49] along with the geometrical quantities that define the vacuum reactor and the transport of species from the target towards the film, such as the target size, the position of the racetrack, the target-film distance, the substrate rotation angle, the pressure in the reactor as well as the temperature, which are dependent on the particular deposition system and conditions. From these input quantities, the SIMTRA code simulates the transport in the gas phase of the species sputtered from the

target until they are deposited at the substrate, thus providing the linear momentum distribution function of the deposition species at the substrate, $f(\vec{p})$. Here, it is important to notice that SIMTRA also provides a list with the kinetic energies and directions of arrival of numerous deposition atoms at the substrate, although due to the important correlation between these quantities, in the proposed model, the momentum vector distribution is again employed instead of two uncorrelated energy and angular distribution functions. $f(\vec{p})$ is then introduced as an input into a home-made Monte Carlo model of the film growth. This code simulates the incorporation of different deposition species on a flat substrate that defines the XY plane, whereas the z axis corresponds to the direction perpendicular to it. The space is then divided into a $N_x \times N_y \times N_z$ cubic grid, where each cell has the value 1 if it contains a deposited species and 0 otherwise. For metals, each cell represents the typical atomic volume in the material, with a typical length of ~ 0.4 nm. The deposition species are considered to approach the substrate from a random initial location over the substrate and to follow a straight trajectory defined by $\vec{p}$, which is randomly calculated using $f(\vec{p})$. Consequently, in the model, the angular distribution that defines the direction of movement and the kinetic energy distribution function of the deposition species are strongly correlated through $f(\vec{p})$. The movement continues in the cubic grid, using periodic boundary conditions in the XY plane, until the arriving species land on the substrate or try to move into an occupied cell. In this latter case, the following processes are considered:

- *Kinetic energy-induced mobility*: If the energy involved in the collision between the arriving and surface atoms, $p^2/2M$, where M is the mass, is above certain energy threshold, ε_k, both atoms are allowed to move into the film network according to a given surface relaxation scheme (see below) [20–22].
- *Biased diffusion*: If the kinetic energy-induced mobility process is inefficient, either because the kinetic energy is below ε_k or because there are no available neighbor sites where to relax, it is considered that the incident atom keeps part of its momentum in the direction parallel to the film surface, $p_\parallel$, and slide over it until it finds an obstacle, where it gets deposited. As stated in [20, 30], this process takes place if the energy associated to that component of momentum, $p_\parallel^2/2M$, is above certain threshold value, ε_{BD}, and the angle of incidence is above certain angular threshold with respect to the normal to the surface, θ_{BD}. Consequently, this process is introduced in the same way as in [30] without alterations.
- If none of the abovementioned processes takes place, the arriving atom is deposited at the landing position and no subsequent mobility processes are considered.

The model is therefore solved by knowing the features of the deposition reactor, the deposition conditions, as well as ε_k, ε_{BD} and θ_{BD} (see figure 1). These quantities were estimated as follows: ε_k was taken as the surface binding energy of the material, estimated as the enthalpy of sublimation, whereas
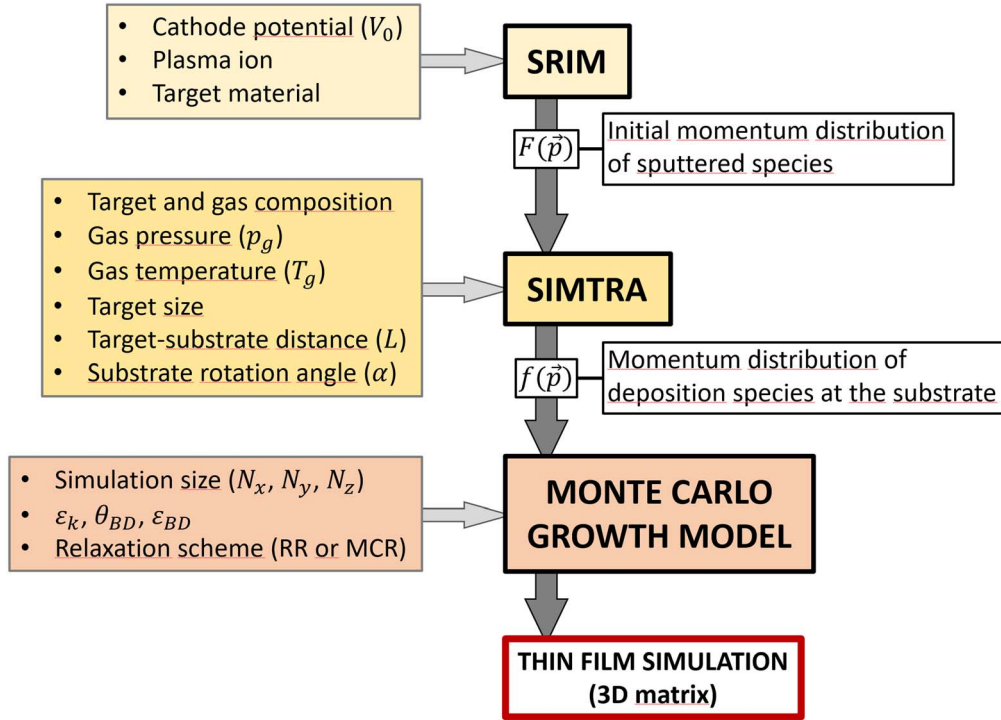
Figure 1. Scheme of the different modules of the growth model, and the different input quantities required to solve it.

the biased diffusion energy and angular thresholds were estimated as $\varepsilon_{BD} \sim 1$ eV and $\theta_{BD} \sim 30°$ [20, 30]. Moreover, the remaining input data in the model have been taken from table 1 (and table S1 in the supplementary material) for each simulation condition. It is important to underline that the model does not contain any aditional input quantity or adjustable parameter, and that it only employs the data explicitly mentioned in this paper as an input. The size of the simulations was $N_x = N_y = 2500$, i.e. a base of ~ 1 μm $\times$ 1 μm, and a value of N_z to match the thickness of the experimental films.

3.2. Surface relaxation schemes

The HT relaxation of the arriving and surface atoms in the film network is a complex phenomenon that involves (i) the breaking of surface bonds, (ii) the interaction of both incoming and surface atoms, and (iii) the mobilization of these atoms (relaxation) on a growing surface to a final position in the surface network, whose detailed analysis is far beyond the scope of this manuscript. Instead, in this paper, a similar approach as in [30] was followed, where a simplified, effective scheme was presented. There, this process is simplified by introducing a so-called relaxation region, which contains all possible neighbor positions where both atoms may migrate to. In [30] it was introduced as a cone-shaped volume with its apex located at the position of the collision, opening angle of $\pi/4$ and its axis aligned with the momentum of the arriving atom. In this way, all neighbor positions both empty and coordinated within this region are considered potential destinations for these atoms (see figure 2 for a 2D illustration of a single relaxation process). Based on this

simple idea, the two following surface relaxation schemes are considered:

- *Random position relaxation (RR)*, where the final destinations of both atoms are randomly chosen among all the positions available in the relaxation region, and
- *Most coordinated position relaxation (MCR)*, where the destinations of both atoms are the two most coordinated positions available in the relaxation region, determined as follows: for each of the positions in the relaxation region, a coordination number is calculated. The relaxing atom will then end at the position with the highest coordination number. In the case that there is more than one position with the same highest coordination number, one of them is randomly picked.

The two surface relaxation schemes described above are introduced *ad-hoc* into the calculations and must be understood as effective processes that combine numerous elemental processes affecting the dynamics of surface atoms. Despite their similarities, these two schemes introduce profound differences in the simulation of the growth dynamics and in the morphological development of the films. In the final part of the paper (section 4.5), and based on the results of the model and their comparison with the experimental data, their physical nature and origin are discussed. However, it is worth to mention that the RR scheme was already implemented in [30, 45] as a basic relaxation mechanism, and, hence, our model is identical to the one employed in these references whenever this scheme is considered. However, the solutions of the model using the MCR scheme are presented and discussed here for the first time.
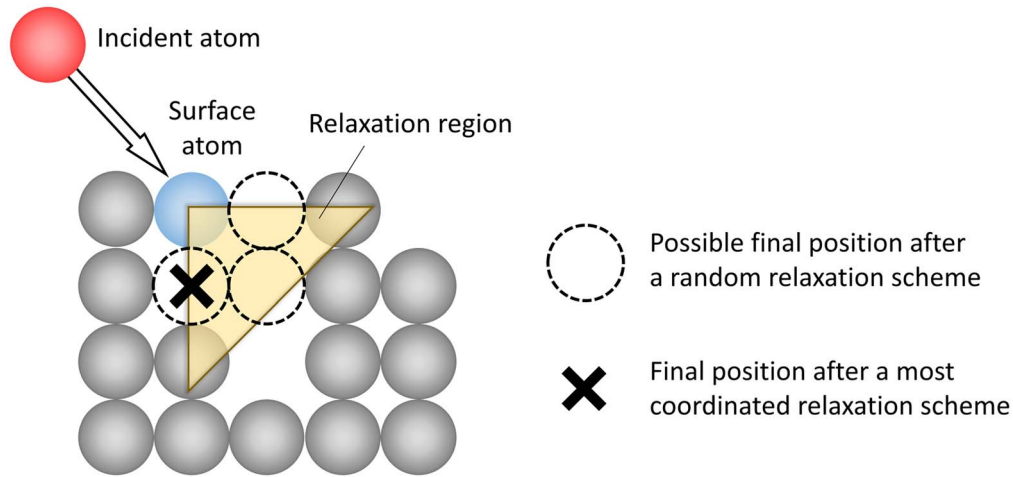
Figure 2. Illustration of the surface relaxation schemes. For clarity reasons, a 2D illustration of a single relaxation process is presented. In the actual model, the relaxation process takes place within a 3D relaxation cone and both atoms (incident and surface atoms) are allowed to relax.
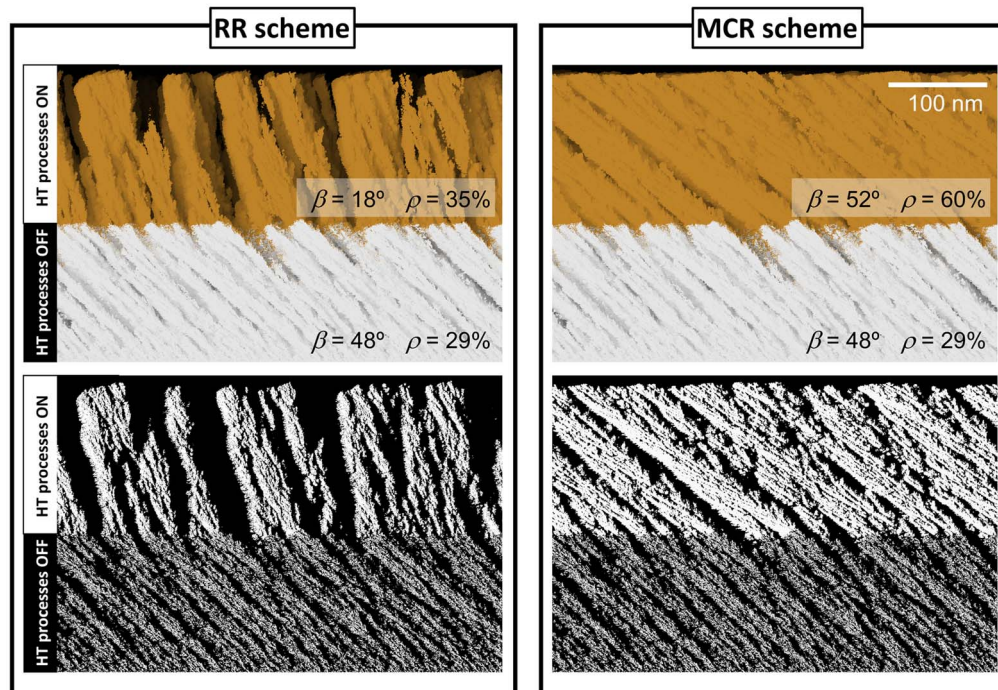

Figure 3. Influence of the HT processes in the results of the model. The simulations correspond to the deposition of Ti, in the conditions of [30], for $\alpha = 80°$, with film thickness of 300 nm. The first 150 nm of growth have been carried out with all HT processes inhibited, and subsequently activated during the remaining 150 nm according to different relaxation schemes. Top images: results of the simulation illustrating the change in density and in tilt angle of the nanocolumns. Bottom images: a one-atom slice of the same simulated material as above, illustrating the influence of HT processes in the porosity.

3.3. Influence of the surface relaxation schemes on the simulations

The introduction of a particular surface relaxation scheme in the simulations strongly influences the calculated results. Actually, the use of a given scheme alters the distribution of empty positions on the film surface and affects the efficiency of other mechanisms, such as the biased diffusion or even surface shadowing processes, the latter responsible for the nanocolumnar growth. In fact, all of them are strongly interdependent, and a variation in one of them results in a completely different growth dynamic and film nanostructure.

In order to illustrate how the use of a particular surface relaxation scheme affects the film nanostructure, a simulation has been run as follows: as a case example, the model has been solved according to the conditions defined in [30] (see third row in table 1) when $\alpha = 80°$ and for a total film thickness of 300 nm. Moreover, in this simulation, all HT processes have been inhibited during the first 150 nm of growth to illustrate the film nanostructure in absence of HT processes and under the solely influence of surface shadowing mechanisms. Subsequently, the HT processes have been activated during the following 150 nm, up to a total film
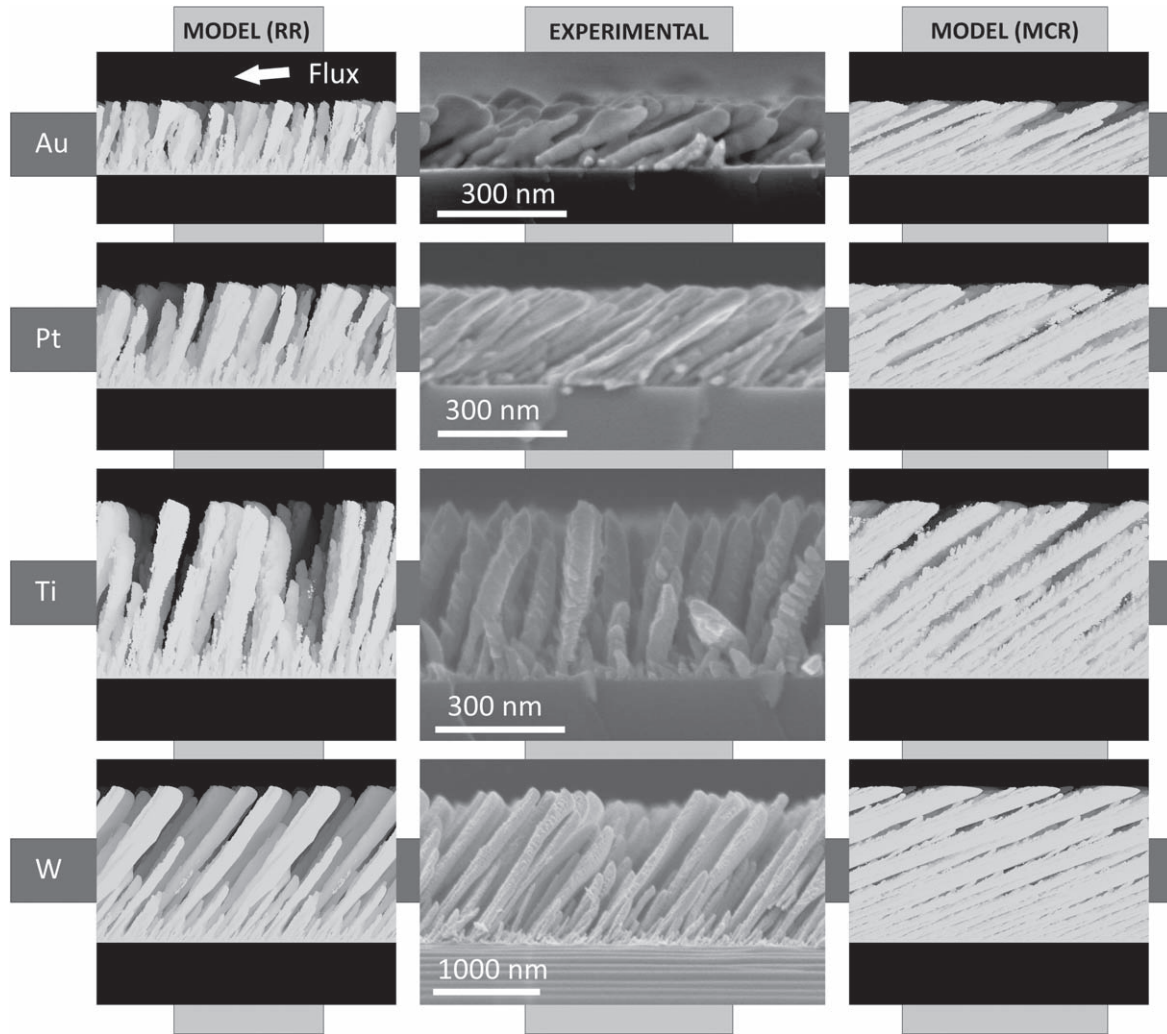
Figure 4. Center) FESEM images of Au, Pt, Ti and W thin films grown by MS-OAD when the angle aligning the racetrack and the substrate is $\alpha_b = 85°$ (i.e. α(Au) = 85°, α(Ti) = 85°, α(Pt) = 90° and α(W) = 100°). Sides) Results of simulations using the two hyperthermal relaxation schemes: Random Relaxation (left) and Most Coordinated Relaxation (right). The arrow indicates the direction of arrival of the deposition flux. Simulations are in the same scale as the experiments.

thickness of 300 nm. The results appear in figure 3: there, typical tilted nanocolumnar structures with $\beta = 48°$ are obtained for thicknesses below 150 nm, with a film density of 29%. Remarkably, when the HT processes are activated according to a RR scheme, columns sharply become more vertical due to the appearance of relaxation processes in the direction of arrival of the deposition species, i.e. in the direction of the incoming momentum, in a process already reported in [30]. This also translates into a small increase of the film density, from 29% to 35% in this region, that is clearly appreciable when showing a 1 cell-depth slice of simulated material (see bottom part of figure 3). Remarkably, when the MCR scheme is imposed, only a slight variation of column tilt angle is noticeable, from $\beta \sim 48°$ to $\beta \sim 52°$. Yet, the film density shifts from 29 % to 60 %, revealing the influence of the surface relaxation processes during growth. This is clearly visible when displaying the 1 cell-depth slice of this simulated material, where the increase of density is noticeable. This suggests that the MCR scheme induces certain surface relaxation dynamics that does not significantly

alter the original growth defined by the surface shadowing mechanisms, leaving the column tilt rather unaffected but making the structures denser. Consequently, the introduction of these two relaxation schemes in the model induces profound changes in the simulated growth dynamics, and affects the columnar development, density and tilt angle.

4. Results and discussion

4.1. Growth of Au, Pt, W and Ti thin films by MS-OAD

The columnar morphology of the Au, Pt, W and Ti thin films is illustrated in figure 4, where the cross-sectional FESEM images of these films for the same angle aligning the racetrack and the substrate $\alpha_b = 85°$ (i.e. for $\alpha(Au) = 85°$, $\alpha(Ti) = 85°$, $\alpha(Pt) = 90°$ and $\alpha(W) = 100°$) are shown. At a glance, important structural differences are apparent despite the similar deposition conditions: Au and Pt nanocolumns are clearly more tilted that those of Ti and W. Moreover, the shape
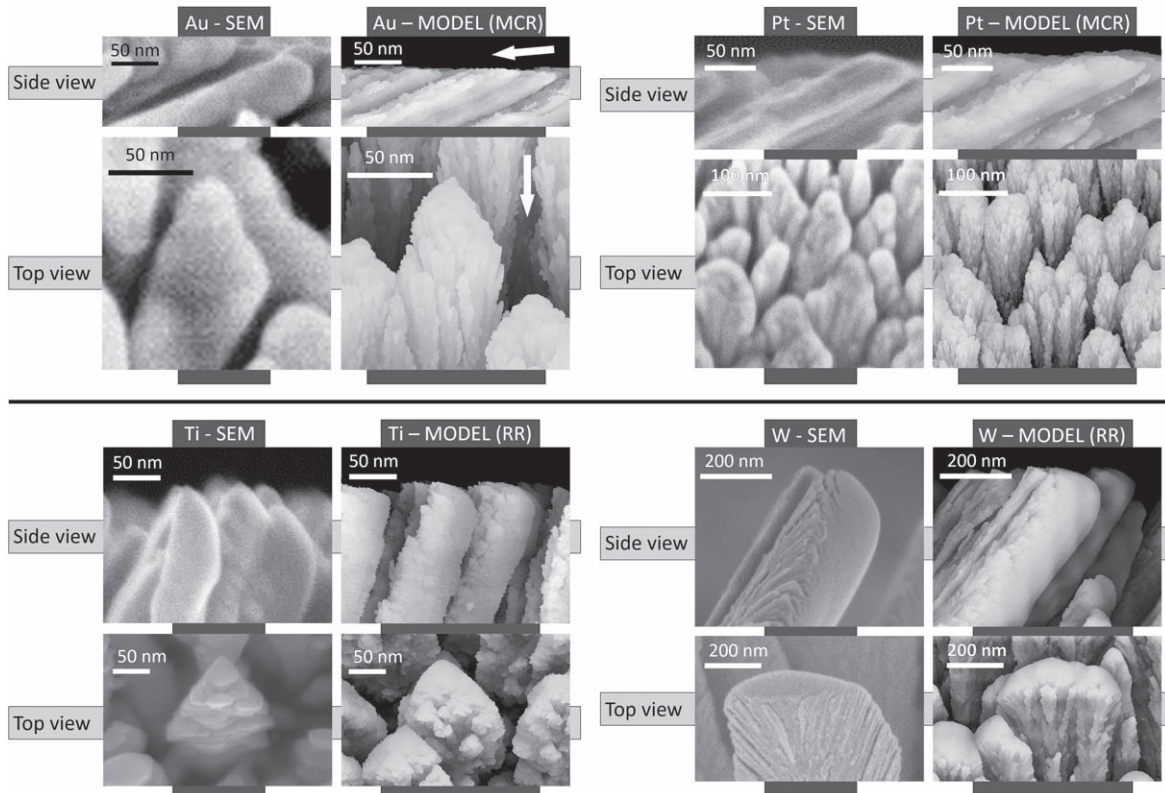
Figure 5. (Top) Cross-sectional and top FESEM images of the tip of the nanocolumns of Au and Pt, along with the results of the simulation according to a most coordinated relaxation scheme. (Bottom) Cross-sectional and top FESEM images of the tip of the nanocolumns of Ti and W, along with the result of the simulation according to a random relaxation scheme. The arrows indicate the direction of arrival of the deposition flux. Simulations are in the same scale as the experiments.

of the nanocolumns is rather different (see detailed cross-sectional and top view images of the nanocolumns in figure 5): while those in the Au/Pt thin films are rather smooth and homogeneous, those in Ti/W present two different sides: a smooth side facing the target and an opposite one that contains some fibrous formations. Also, Ti and W nanocolumns possess a peculiar and distinctive tip with respect to Au and Pt: the cross-section images of Au/Pt in figure 5 show that the tips are rather symmetric with respect to the column axis, while in the case of Ti/W these present a finger-like shape, with a curved side facing the target and a rather flat and fibrous surface at the back side. In this regard, the existence of W columns deposited by MS-OAD with different morphology on either side was already reported in [45], in agreement with the results shown here. Consequently, remarkable similarities have been found between the nanocolumnar morphologies of Ti and W, on one hand, and of Au and Pt on the other hand.

In figure 6 we show the values of β and ρ for the whole set of Au, Pt, Ti and W thin films as a function of α. Overall, ρ shows a common trend in all the cases, with decreasing values when α increases. However, there is an important difference between these materials regarding the relation between α and β: for Au and Pt, β shows an increasing trend with α, reaching values up to $\beta \sim 60°$ when $\alpha \sim 90°$, while for Ti and W the value of β seems rather constant for $\alpha > \sim 30°$ with values of β below 35°. Therefore, the results in figures 4, 5 and 6 suggest the existence of two different columnar growth modes: one for Au and Pt and another for Ti

and W. This is more noticeable in figure 7 where we display the value of β as a function of ρ for Au, Pt, W and Ti taken from figure 6, and where two clear and distinct trends are evident: for Au/Pt the values of β decrease with ρ following a smooth decay when $\rho < 90\%$ and a steep decay when $\rho > 90\%$. In the case of Ti/W, on the other hand, when $\rho < 70\%$, β and ρ smoothly increase, until β reaches a maximum when $\rho \sim 70\%$, above which β progressively falls. Consequently, all the evidence suggests the existence of two types of growth, the first one obtained for Au and Pt and the second one for Ti and W thin films, which result in different columnar tilt, morphology and film density.

4.2. Growth modes and surface relaxation schemes

To understand the origin of the two growth modes found above, we have solved our model for Au, Pt, Ti and W using the experimental conditions listed in table 1, and using the two relaxation schemes described in section 3. The cross-sectional views of the simulated films for $\alpha_b = 85°$ (i.e. for $\alpha(\text{Au}) = 85°$, $\alpha(\text{Ti}) = 85°$, $\alpha(\text{Pt}) = 90°$ and $\alpha(\text{W}) = 100°$) are depicted in figure 4 for Au, Pt, Ti and W. Remarkably, the solution under a RR scheme seems to appropriately describe the morphology of the W and Ti thin films, not only regarding the general aspect of the nanocolumns and tilt angle, but even the existence of smooth and fibrous sides of the nanocolumns and the characteristic tip. This is evident in figure 5, where a detailed image of a W and a Ti nanocolumn are displayed, along with a
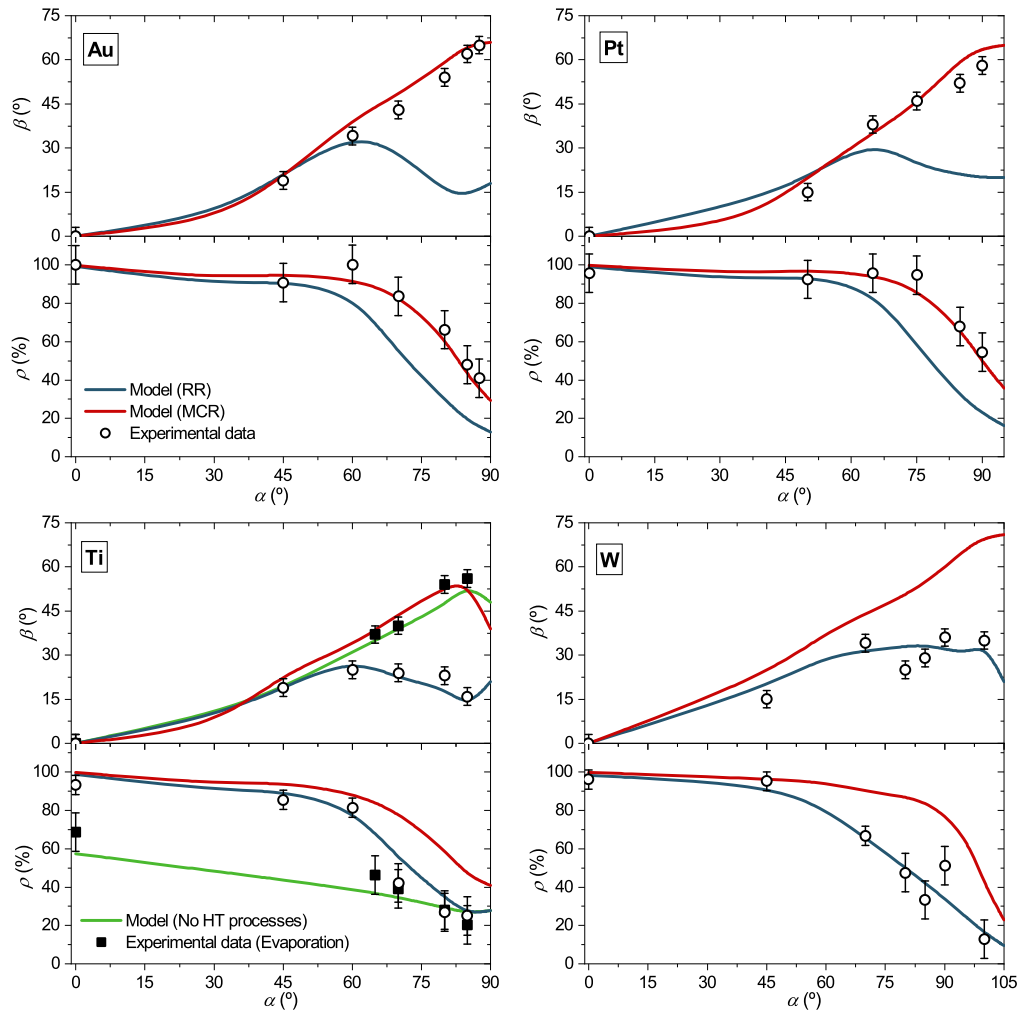
Figure 6. Values of the tilt angle, β, and density, ρ, of Au, Pt, Ti and W thin films deposited at different substrate rotation angles, α. The results of the simulations when following a Random Relaxation or Most Coordinated Relaxation schemes are included as lines after spline interpolation. In the case of Ti, the experimental values of β and ρ as a function of α when using the evaporation technique are also included, along with the results of the simulations in the absence of HT processes.

zoomed view of the calculated morphology when using a RR scheme. Furthermore, the solutions of the model when using a MCR scheme in figure 4 do not yield good results regarding the W/Ti films, although they remarkably reproduce quite well the morphology of the Au/Pt thin films, the tilt angle of the nanocolumns, their morphology and the characteristical shape of the tip (see figure 5 for a zoomed view of the simulations and a comparison with the experimental images).

The model described in section 3 was solved for increasing values of α, with a 5° interval, under the conditions defined in table 1 for Au, Pt, Ti and W films, and for both surface relaxation schemes. Afterwards, the relative film density and the column tilt angle were calculated from the numerical simulations provided by the model. The adequacy of the model to describe the growth of Au/Pt and W/Ti thin films is evidenced in figure 6 where, along with the experimental values of β and ρ as a function of α, the solutions of the model under each surface relaxation scheme are included as spline lines. In agreement with the previous result, it is clear that the solutions using the RR scheme compare fairly well with the experimental values found for Ti and W, while

the solutions using a MCR scheme match the experimental values for Au and Pt. The calculated results are also included in figure 7, demonstrating the adequacy of each relaxation scheme to describe the two reported growth modes (the dispersion of the experimental data with respect to the calculated values under the adequate scheme is under 5° in the case of β and 10% in the case of ρ). For clarity purposes, in this figure, a single curve for W and Ti, calculated as the average between both solutions when employing the RR scheme is plotted, along with another curve calculated similarly for Au and Pt when using the MCR scheme. Moreover, the shadowed region along the lines represents the dispersion of the calculated data when performing the average. In this way, the accuracy of the model to reproduce tilt angle, nanocolumnar morphology and film density in all studied cases strongly suggests that the growth dynamics stems from the competition of surface shadowing mechanisms along with HT processes under different surface relaxation schemes.

As mentioned in the introduction, a relevant aspect in this analysis concerns the comparison between the nanocolumnar growth in MS-OAD and in evaporation. For this, Ti thin films
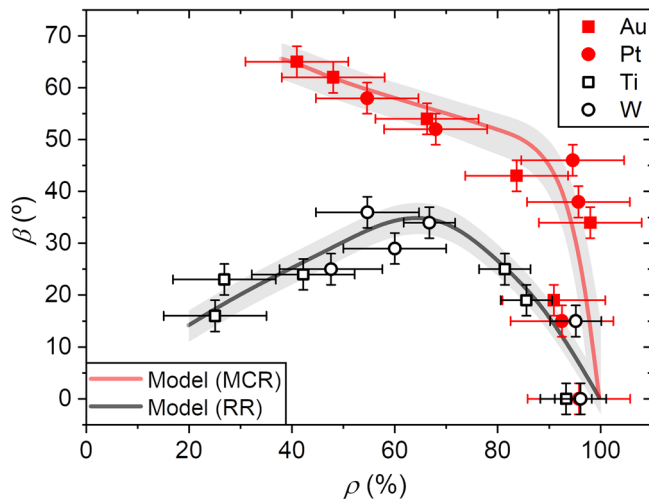
Figure 7. Column tilt angle, β, as a function of the film density, ρ, for Au, Pt, Ti and W. The red thick line represents the solution of the model, averaged for Au and Pt, when following the Most Coordinated Relaxation scheme, while the associated shadowed region represents the dispersion of each particular solution. The black thick line and the associated shadowed region represent the same for Ti and W when the model is solved using the Random Relaxation scheme.

have been deposited by evaporation at glancing angles (see section 2): the experimental values of β and ρ for the evaporated films as a function of α are plotted in figure 6, where the solutions of the model for MS-OAD in absence of any HT processes are included. There, it is clear that this latter calculation reproduces relatively well the values of β and ρ for these evaporated films, which is coherent with the fact that, (i) the geometrical arrangement in the magnetron sputtering reactor and in the evaporation setup is quite similar, and that (ii) due to the specifics of evaporation, the deposition species possess low kinetic energies and, hence, cannot trigger HT mechanisms. Remarkably, a good agreement between the experimental values of β as a function of α and the solutions of the model under a MCR scheme is found, although, in terms of density, the results are not satisfactory, which implies that the evaporation and the MS-OAD techniques promote completely different growth dynamics, in agreement with [29] and the results in section 3.3. Interestingly, this explains why many articles in the literature successfully apply phenomenological relations deduced for the evaporation technique to estimate the value of β in MS-OADs (e.g. the so-called tangent or cosine rules [32]). Yet, any other morphological aspect, e.g. film density or columnar shape, clearly differ, suggesting that, in general terms, this positive result must be taken as coincidental. Moreover, it also explains why a model that does not include any HT mechanism is able to accurately calculate the tilt angle of Au nanocolumns in [37].

4.3. Surface relaxation schemes in experimental data taken from the literature

In order to perform a complete analysis on the existence of the two growth modes and their connection with the surface relaxation schemes, numerous experimental data taken from the literature on different materials grown by MS-OAD are analyzed next. With the exception of some specific cases on TiO$_2$ [38] and Cr [39], only the value of β as a function of the deposition conditions is generally reported. Therefore, this analysis is divided in two parts, the first one focused on the two abovementioned materials, whereas in the second we have only studied the values of β as a function of the deposition conditions for many other materials.

In figure 8 we plot the values of β and ρ as a function of α for TiO$_2$ taken from [38] and Cr taken from [39] along with the solutions of the model according to each relaxation scheme (input data taken from table 1). At a glance, it is remarkable that both model solutions are rather close to each other, especially in the case of Cr: this is caused by the higher value of the deposition pressure that leads to a relatively short mean free path of sputtered species in the plasma gas and, hence, to a loss of kinetic energy before their deposition and a decreasing influence of HT processes during growth, making both solutions of the model quite similar. Actually, this explains why the two proposed relaxation schemes have not been previously detected in the literature, as they only become evident under very low-pressure conditions and when the target-film distance is rather short, i.e. when there is a relevant number of deposition species arriving at the film with sufficient kinetic energy to trigger HT processes. In any case, the experimental results on TiO$_2$ seem to better follow the model solved under a MCR scheme, while, for Cr, the two solutions are so close that no conclusions can be drawn. Nevertheless, the solutions of the model provide good estimations of the experimental values of β and ρ in both cases (note that the density in the case of Cr was estimated using the x-ray reflectivity technique at grazing incidence in [39]).

In figure 9, a chart graph with the experimental values of β taken from the literature is shown. In particular, on Al, Cr and Ti [32], HfN [40], Ti and Mo [41], Ti [31], V [42, 43], WO$_3$ [44], and W [45, 46], grown by MS-OAD in the conditions described in section 2. In that figure, the calculated values of β when solving the model in their respective experimental conditions, when considering the MCR and RR schemes, have also been included (the input data employed in the simulations are detailed in table S1 in the supplementary material). In all the cases, it is appreciated the good agreement between experimental data and one of the solutions of the model, which corroborates the existence of the two growth modes introduced above. For WO$_3$, Cr, Al, Mo and V, for instance, we find that the values of β are well reproduced by the model when using a MCR scheme, while the W and HfN cases seem to be better described using a RR scheme, in agreement with the experimental results presented above. In this way, and based on figures 4–9, it might primarily seem that the prevalence of a given relaxation scheme over the other is linked to the chemical nature of the material. However, the analysis of the data presented for Ti in figure 9 introduces an important paradigm: there, the Ti films taken from [31] clearly grow following a MCR scheme, with values of β above 50°, whereas those taken from [32] and those in figure 4 seem to grow following a RR scheme, with values of β rather constant and below 30° no matter the value of α. This
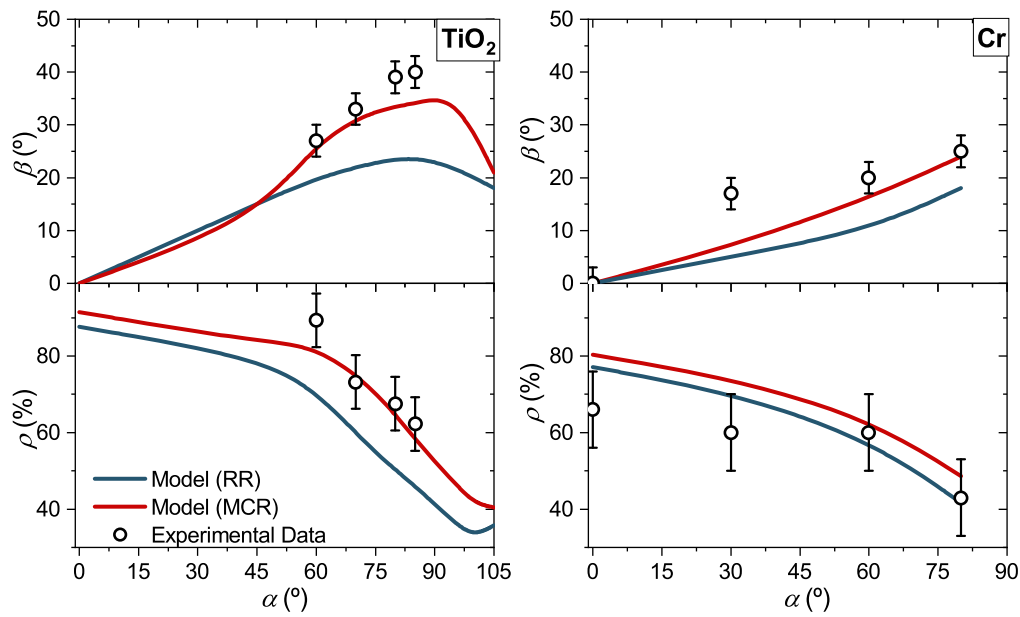
Figure 8. Column tilt angle, β, and density, ρ, as a function of the substrate rotation angle, α, for TiO$_2$ and Cr thin films deposited at intermediate pressures, taken from [38] and [39], respectively. The results of the simulations when following the two HT relaxation schemes are included as lines after spline interpolation.
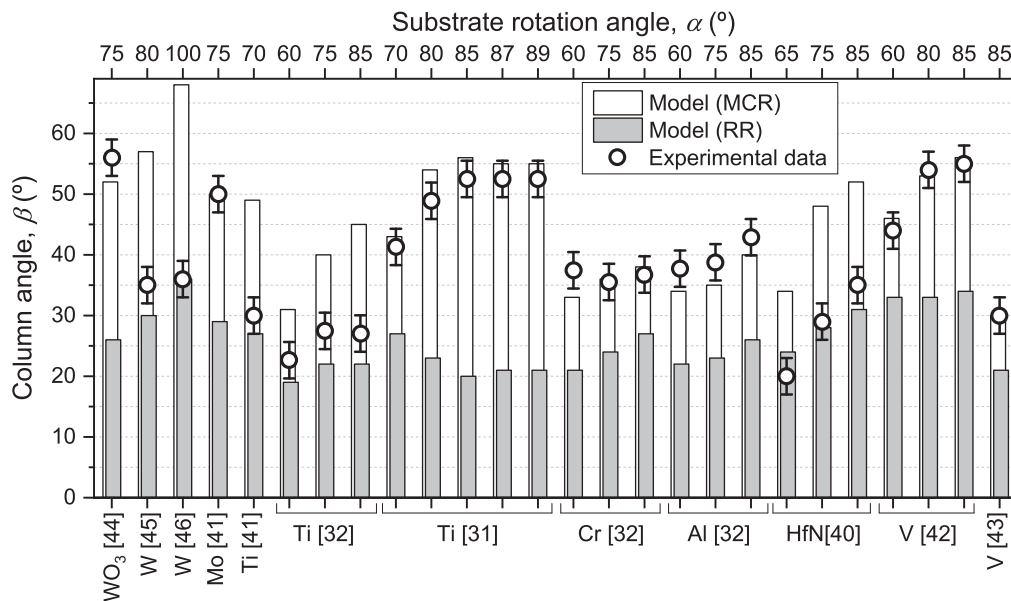

Figure 9. Tilt angle of the nanocolumns, β, for different materials and MS-OAD conditions taken from the literature (data points). The bottom *x*-axis indicates the film composition and the reference from where the data were taken. The top *x*-axis indicates the substrate rotation angle as reported in the corresponding reference. Columns indicate the calculated value from the model, solved in the respective experimental conditions using either HT relaxation scheme.

has profound implications, as it seems that, in addition to the chemical nature of the material, the experimental conditions may determine whether the surface relaxation follows a given scheme and, therefore, that there must be a transition between modes when varying experimental parameters. This is further supported by analyzing the growth of Ti and W films in figure 6, which follow a RR scheme, in comparison with that of TiO$_2$ (figure 8) and WO$_3$ (figure 9), which follow a MCR scheme, suggesting that the sole addition of oxygen into the films alters the surface relaxation scheme. Actually, and even

though this issue will be studied in detail in the future, it is possible that this transition takes place even when the oxygen content in the growing film is very low, which could imply a direct relation between the residual oxygen in the deposition reactor and the growth mode.

4.4. Transition between surface relaxation schemes

Based on the results above and the straightforward relation between experimental conditions and growth modes in Ti, we
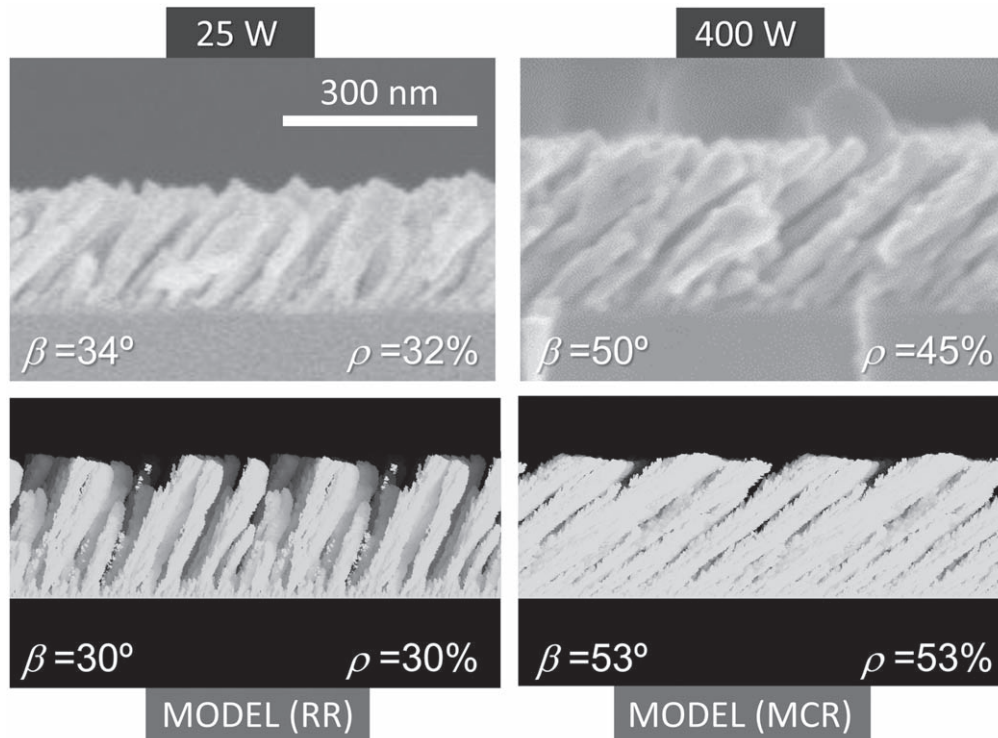
Figure 10. FESEM images of a Ti thin film deposited using a DC power of 25 W (left) and 400 W (right). Below, the solutions of the simulations when following either HT relaxation scheme. Values of the column tilt angle, β, and film density, ρ, are also included.

now analyze which experimental quantity may determine the particular surface relaxation scheme, and whether such transition takes place sharply or smoothly. For this, we analyze some results in the literature on the MS-OAD of Ti thin films that report a smooth change in β and ρ when solely varying the DC power employed to maintain the plasma discharge, P_w, which from now forth we simply dub *power*, from $P_w = 25$ W to $P_w = 400$ W. In this way, in [29] it was demonstrated that this morphological transition was not caused by any thermally-induced effect or by any other well-known atomistic mechanism. However, as mentioned above, the presence of residual oxygen in the deposition reactor could potentially influence the relaxation scheme, and ultimately the oxygen content in the film due to the strong dependence of the deposition rate of Ti with power. This analysis is presented in the supporting information (figure S1), where a Nuclear Reaction Analysis of these layers was carried out, indicating that the ratio O/Ti is rather constant and around 0.7, most likely due to the post-deposition exposure of these layers to atmospheric oxygen. Consequently, any likely variation of the O/Ti ratio with power must be constrained between 0 and 0.7.

The adequacy of the RR scheme to describe the growth of the Ti films when $P_w = 25$ W was already demonstrated in [29]. Consequently, and under the light of the results presented above, it is now studied whether the MCR scheme could be involved in this morphological transition. In figure 10, the cross-sectional SEM images of the Ti films grown in [29] with $P_w = 25$ W and $P_w = 400$ W, respectively, are presented, where the values of β and ρ in either

case are included. Below these images, the solutions of the model using the two relaxation schemes are displayed (the input data to solve the model are presented in table 1): in agreement with [29], the solution using the RR scheme compares well with the $P_w = 25$ W case, with similar morphology and values of β and ρ. Remarkably, the solution of the model when using the MCR scheme reproduces well the experimental values when $P_w = 400$ W, with a deviation of $\sim 3°$ in β and $\sim 8\%$ in ρ. In figure 11 we display both, β versus α and ρ versus α corresponding to the whole set of films presented in [29] as a function of power, along with two horizontal lines corresponding to the two solutions of the model. In this way, the good agreement between the results of the model and the experimental data when $P_w = 25$ W and $P_w = 400$ W suggests that, as a plausible hypothesis, this morphological transition with power could be linked to a change in the surface relaxation scheme. Moreover, it is remarkable the smooth change in β and ρ with power from one relaxation scheme to the other, therefore suggesting a smooth shift between both surface relaxation schemes for the intermediate cases. This would imply the existence of hybrid relaxation schemes in which both schemes coexist. To check this possibility, we have performed a mathematical exercise by introducing a new input parameter into the model, χ_{MCR}, defined as the fraction of HT relaxation processes that follow a MCR scheme during growth, operating as follows: when a HT relaxation process takes place in the simulations, a random number is generated between 0 and 1 and compared with χ_{MCR}. If it is lower, the relaxation will follow a MCR scheme; otherwise, it will follow a RR scheme (note that the fraction
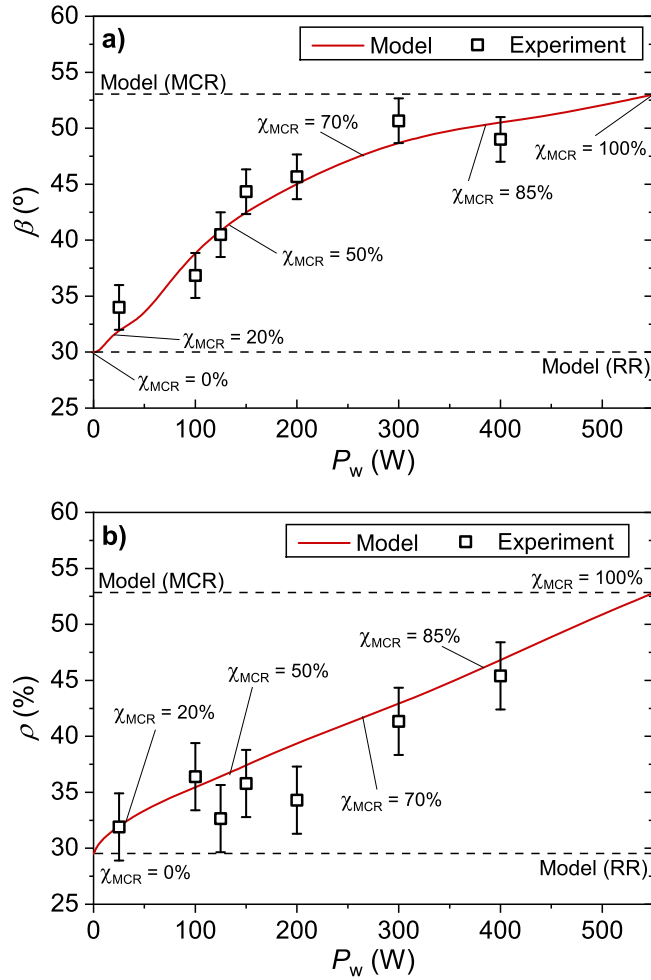
Figure 11. Ti column tilt angle, β, (a) and film density, ρ, (b) as a function of the DC power, P_w, taken from [29]. The solutions of the model when following either relaxation scheme are included as horizontal lines. The solutions when smoothly changing the fraction of Most Coordinated Relaxation schemes, χ_{MCR}, are included when assuming the relation $\chi_{MCR} = 0.043 \times P_w^{1/2}$ (W$^{-1/2}$).

of random relaxation schemes during growth, χ_{RR}, would be $\chi_{RR} = 1 - \chi_{MCR}$). In this way, the value of χ_{MCR} as a function of power to reproduce the experimental data has been estimated by performing a mathematical fit: the calculated values of β and ρ as a function of power have been depicted in figure 11 when the relation $\chi_{MCR} = 0.043 \times P_w^{1/2}$ (W$^{-1/2}$) is considered, which allows for a fairly good agreement in all the cases. This is also shown in figure 12, where the experimental values of β versus ρ are displayed, along with a solid line corresponding to the solutions of the model, indicating the adequacy of our calculations to reproduce the experimental data. However, this conclusion must be understood as a result of a purely mathematical exercise to check whether the smooth structural transition with power could be explained by means of a smooth transition between surface relaxation schemes. Nevertheless, this positive result does not ensure the adequacy of the hypothesis and, hence, the origin of the structural shift with power reported in [29] is yet to be fully explained.
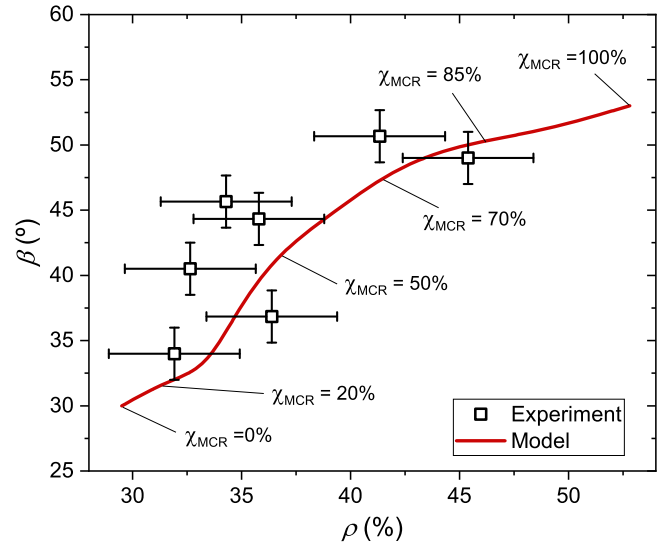

Figure 12. Experimental data (taken from [29]) and calculated values of the column tilt angle, β, as a function of the film density, ρ, when assuming the relation $\chi_{MCR} = 0.043 \times P_w^{1/2}$ (W$^{-1/2}$).

4.5. On the origin of the two surface relaxation schemes

It is important to notice that, in this paper, the two surface relaxation schemes have been introduced ad hoc to explain the vast amount of experimental casuistic in the literature, and that their physical meaning or origin has not yet been discussed. This is carried out next, although giving a straight and conclusive answer to these issues is far beyond the scope of this paper. Actually, any Monte Carlo model describing the thin film growth includes a series of mechanisms that are usually developed from a more fundamental physical description, such as molecular dynamics or first principles approaches, so those mechanisms clearly represent a given physical phenomenon. However, the analysis in this work follows a rather different approach, as a new mechanism has been directly introduced into a Monte Carlo simulation in an attempt to understand different experimental data, without any prior fundamental calculation backing it up. Consequently, the proposed relaxation schemes do not represent elemental atomistic mechanisms but, instead, effective processes that allow to mimic the growth dynamics of experimental thin films.

From a physical point of view, and solely attending to their definition, it is clear that the main difference between the two proposed relaxation schemes relates to the way the surface atoms locally relax in the film network after an initial knock-on collision and, in particular, to whether these atoms move towards most stable locations from an energetic point of view (i.e. most coordinated positions) or not. Actually, and based on this simple idea, the proposed model accurately reproduces (i) the transition compact/nanocolumnar, (ii) the tilt angle of the nanocolumns, (iii) the typical column diameter, (iv) the appearance of certain patterns on the surface of the nanocolumns, (v) the shape of the tips of the nanocolumns, and (vi) the film density, all of them for different rotation angles of the substrate and for different materials

deposited under numerous and different conditions, some of them carried out specifically for this paper and others taken from the literature. This evidence strongly suggests that, no matter whether the two relaxation schemes represent elemental processes or effective mechanisms, the model accurately reproduces the growth dynamics of the studied nanocolumnar thin films under the conditions explained in the experimental section. Moreover, it is also found that when the HT processes are switched off in the model, the solutions reproduce the morphology of evaporated thin films, suggesting that the model is physically coherent.

Based on the ideas above, and on the fact that each surface relaxation scheme may involve the confluence of many elemental processes, we postulate the following hypothesis to rationalize the presented results: *while the HT process is triggered in a first (knock-on) stage caused by the arrival of deposition species at the film surface with relatively high kinetic energies, the relaxation scheme represents a subsequent process mediated by the state of the growing film surface, which conditions whether the atoms involved end up at most energetically stable locations or not.* This is in line with the experimental results presented in [50, 51], where Shaginyan *et al* found that increasing values of the energy flux towards the film in classical magnetron sputtering depositions promoted the formation of a so-called hot thin solid layer on the top of the growing surface that modifies the way gaseous atoms get deposited, from a classic gas → solid to a gas → liquid → solid scheme, in a clear parallelism with our results. Moreover, this would explain why an increase of power involves a transition in the surface relaxation scheme in the case of Ti, as this quantity greatly influences the energy flux towards the film during growth [52].

The proposed hypothesis above also agrees with current ideas on the influence of the normalized energy and momentum fluxes towards the film during growth: as mentioned in the introduction, these fluxes are known for causing mobility of surface atoms and for affecting the film nanostructuring in magnetron sputtering depositions in classical non-oblique geometries. In our case, the introduction of a particular surface relaxation scheme produces particular growth dynamics: under a RR scheme, the movement of the atoms in the film network takes place in the preferential direction of the momentum of the deposition species in the gaseous phase, being the most remarkable effect the straightening up of the nanocolumns, while the film density changes very little. Under a MCR scheme, on the other hand, the relaxation seems to adapt to the growth direction defined by the surface shadowing mechanisms, causing the densification of the nanocolumns and a slight variation in the tilt angle. Therefore, from a global perspective, our model obtains a 'momentum-driven relaxation process', linked to relaxation processes in the preferential direction of the incoming momentum of the deposition species, or an 'energy-driven relaxation process', linked to an increase of the film density and of the coordination of the deposited atoms. These results are in line with those found in [23], where the influence of the normalized momentum and energy fluxes are described.

Given the analysis above, one would think that the logical next step is the study of the surface relaxation schemes by means of Molecular Dynamics or First Principles simulations. However, these approaches are not evident due to the lack of specific quantitative information on different phenomena, such as the appearance of the hot thin solid layer or the influence of the energy/momentum fluxes on the film growth. Actually, these phenomena encompass numerous elemental processes and mechanisms at an atomic level that promote a collective behavior of the surface atoms, and that end up causing specific growth dynamics. In this regard, the model presented here proposes a set of mechanisms, either elemental or effective, that quantitatively reproduce this growth dynamic for numerous thin films in scales of tens of nanometers, thus shedding some light on the different surface phenomena affecting the film growth. Yet, it is worthy to mention that the model does not explain structural features in atomic scales, such as crystalline orientation or film stress, or whether the surface relaxation schemes represent transient or thermal mobility processes [53].

An interesting aspect regarding the physical coherence of the proposed hypothesis relies on the potential existence of a structural transition between relaxation schemes for materials other than Ti. Yet, typical operational range of magnetron sputtering conditions may restrain the appearance of a transition. To study this phenomenon, W thin films have been explicitly grown for this work at higher powers than those presented in figure 6, but no structural transition could be found. The same occurs for Pt, where the deposition system was operated at the lowest possible power to maintain the plasma, but no structural transition was found either in comparison with the cases presented in figure 6. Yet, it is remarkable that, while W and Ti seem to follow a RR scheme in figure 6, the WO_3 and TiO_2 films reported in figure 9 do follow a MCR scheme. This suggests that, as mentioned above, the oxidation process of W and Ti atoms during growth alters the relaxation scheme, in a phenomenon that will be studied in the future.

5. Conclusions

Morphological aspects, such as column tilt angle, column shape and film density of numerous nanocolumnar materials grown by the magnetron sputtering technique at oblique angles at low pressures and temperatures have been compared, demonstrating the existence of two distinct growth modes. With the help of a well-accepted deposition model, these changes have been linked to two different effective surface relaxation schemes upon the arrival of deposition species with kinetic energies above the surface binding energy. From an experimental point of view, we have primarily employed four different materials to illustrate the phenomenon: Au, Pt, Ti and W grown under different conditions and reactor configurations. The first relaxation scheme has been dubbed Random position Relaxation, and accurately explains the main features of films such as W or Ti, while the second scheme has been dubbed Most Coordinated position

Relaxation, and explains the features of films such as Pt or Au. Moreover, it has also been demonstrated that the materials grown by magnetron sputtering are very different to those grown by evaporation, i.e. in absence of hyperthermal processes. Furthermore, the analysis of numerous additional cases taken from the literature on materials as different as Au, Pt, Ti, Cr, TiO_2, Al, HfN, Mo, V, WO_3 and W, grown by MS-OAD in different conditions and reactors, is congruent with the existence of the two proposed effective surface relaxation schemes. Remarkably, this analysis demonstrates that Ti may grow following either one scheme or the other, indicating that the dominating surface relaxation scheme is not only linked to the chemical nature of the material but also to the deposition conditions.

Furthermore, data in the literature regarding a structural transition of nanocolumnar Ti deposited by magnetron sputtering at oblique angles when increasing the DC power employed to maintain the sputter plasma have been studied. Based on this analysis, it has been found that this transition can be explained by introducing a smooth and progressive shift between surface relaxation schemes. A discussion has been carried out on the main features of these relaxation schemes and their influence on the morphology of the growing films. Based on these results, a hypothesis has been put forward on the nature of the surface relaxation mechanism linking it with the state of surface atoms. The obtained results are in line with experimental data in the literature regarding the influence of the normalized energy and momentum fluxes on the film nanostructure, or the appearance of a hot thin solid layer during growth. Overall, and based on the two surface relaxation schemes defined in this paper, a plausible hypothesis that explains the growth of numerous materials under a wide number of experimental conditions has been put forward.

Acknowledgments

Data availability statement

The data cannot be made publicly available upon publication because they are not available in a format that is sufficiently accessible or reusable by other researchers. The data that support the findings of this study are available upon reasonable request from the authors.

ORCID iDs

R Alvarez https://orcid.org/0000-0002-1749-4946
A Garcia-Valenzuela https://orcid.org/0000-0002-5238-6465
V Rico https://orcid.org/0000-0002-5083-0390
J M Garcia-Martin https://orcid.org/0000-0002-5908-8428
A R Gonzalez-Elipe https://orcid.org/0000-0002-6417-1437
A Palmero https://orcid.org/0000-0002-1100-6569

References

[1] Barranco A, Borras A, Gonzalez-Elipe A R and Palmero A 2016 *Prog. Mater Sci.* **76** 59
[2] Godinho V, Moskovkin P, Alvarez R, Caballero-Hernández J, Schierholz R, Bera B, Demarche J, Palmero A, Fernandez A and Lucas S 2014 *Nanotechnology* **25** 355705
[3] Louloudakis D, Kyriakos M, Gil-Rostra J, Koudoumas E, Alvarez R, Palmero A and Gonzalez-Elipe A R 2021 *Electrochim. Acta* **376** 138049
[4] Martin M, Salazar P, Alvarez R, Palmero A, López-Santos C, González-Mora J L and González-Elipe A R 2017 *Sensors Actuators*B **240** 37
[5] Ollitrault J, Martin N, Rauch J Y, Sanchez J B and Berger F 2015 *Mater. Lett.* **155** 1
[6] Sengstock C, Lopian M, Motemani Y, Borgmann A, Khare C, Buenconsejo P J S, Schildhauer T A, Ludwig A and Koller M 2014 *Nanotechnology* **25** 195101
[7] Yoo Y J, Lim J H, Lee G J, Jang K I and Song Y M 2017 *Nanoscale* **9** 2986
[8] Liu Y, Zhao Y, Feng Y, Shen J, Liang X, Huang J, Min J, Wang L and Shi W 2016 *Appl. Surf. Sci.* **363** 252
[9] Polat D B and Keles O 2015 *Thin Solid Films* **589** 543
[10] Lee Y J, Yang Z P, Lo F Y, Siao J J, Xie Z H, Chuang Y L, Lin T Y and Sheu J K 2014 *APL Mater.* **2** 056101
[11] Vitrey A, Alvarez R, Palmero A, González M U and García-Martín. J M 2017 *Beilstein J. Nanotechnol.* **8** 434–9
[12] Troncoso G, Garcia-Martin J M, Gonzalez M U, Morales C, Fernandez-Castro M, Soler-Morala J, Galan L and Soriano. L 2020 *Appl. Surf. Sci.* **526** 146699
[13] Zheng J, Ren X, Hao J, Li A and Liu W 2017 *Appl. Surf. Sci.* **393** 60–6
[14] Zheng J, Lv Y, Xu S, Han X, Zhang S, Hao J and Liu W 2017 *Mater. Des.* **113** 142–8
[15] Lopez-Santos C, Alvarez R, Garcia-Valenzuela A, Rico V, Loeffler M, Gonzalez-Elipe A R and Palmero A 2016 *Nanotechnology* **27** 395702
[16] Depla D and Mahieu S 2008 *Reactive Sputter Deposition (Springer Series in Materials Science)* (Springer) (https://doi.org/10.1007/978-3-540-76664-3)

[17] Depla D 2020 *Magnetrons, Reactive Gases and Sputtering* ed D Depla (North Carolina: Lulu) http://hdl.handle.net/1854/LU-4239033

[18] Garcia-Valenzuela A, Alvarez R, Rico V, Cotrino J, Gonzalez-Elipe A R and Palmero A 2018 *Surf. Coat. Technol.* **343** 172

[19] Alvarez R *et al* 2019 *Nanomaterials* **9** 1217

[20] Kools J C S 2005 *J. Vac. Sci. Technol.* A **23** 85–9

[21] Zhou X W and Wadley H N G 1999 *Surf. Sci.* **431** 42–57

[22] Zhou X W and Wadley H N G 1999 *Surf. Sci.* **431** 58–73

[23] Mahieu S and Depla D 2009 *J. Phys. D: Appl. Phys.* **42** 053002

[24] Welzel T and Ellmer K 2013 *J. Phys. D: Appl. Phys.* **46** 315202

[25] Thomann A-L, Caillard A, Raza M, El Mokh M, Cormier P A and Konstantinidis S 2019 *Surf. Coat. Technol.* **377** 124887

[26] Xia J, Liang W, Miao Q and Depla D 2018 *Appl. Surf. Sci.* **439** 545

[27] Abadias G, Leroy W P, Mahieu S and Depla D 2013 *J. Phys. D : Appl. Phys.* **46** 055301

[28] Cormier P-A, Balhamri A, Thomann A-L, Dussart R, Semmar N, Lecas T, Snyders R and Konstantinidis S 2014 *Surf. Coat. Technol.* **254** 291

[29] Alvarez R, Garcia-Valenzuela A, Rico V, Garcia-Martin J M, Cotrino J, Gonzalez-Elipe A R and Palmero A 2019 *Nanotechnology* **30** 475603

[30] Alvarez R, Garcia-Martin J M, Garcia-Valenzuela A, Macias-Montero M, Ferrer F J, Santiso J, Rico V, Cotrino J, Gonzalez-Elipe A R and Palmero A 2016 *J. Phys. D: Appl. Phys.* **49** 045303

[31] Dervaux J, Cormier P-A, Moskovkin P, Douheret O, Konstantinidis S, Lazzaroni R, Lucas S and Snyders R 2017 *Thin Solid Films* **636** 644

[32] Siad A, Besnard A, Nouveau C and Jacquet P 2016 *Vacuum* **131** 305

[33] Medina-Cruz D, Gonzalez M U, Tien-Street W, Fernandez-Castro M, Vernet-Crua A, Fernandez-Martinez I, Martinez L, Huttel Y, Webster T J and Garcia-Martin J M 2019 *Nanomed. Nanotechnol. Biol. Med.* **17** 36

[34] Thornton J A 1974 *J. Vac. Sci. Technol.* **11** 666

[35] Thornton J A 1975 *J. Vac. Sci. Technol.* **12** 830

[36] Mayer M 1997 SIMNRA User's Guide, Tech. Rep. IPP 9/113, Max-Plank-Institut fur Plasmaphysik, Garching, Germany

[37] Alvarez R, Garcia-Martin J M, Macias-Montero M, Gonzalez-Garcia L, Gonzalez J C, Rico V, Perlich J, Cotrion J and Gonzalez-Elipe A R 2013 *Nanotechnology* **24** 045604

[38] Alvarez R, Lopez-Santos C, Ferrer F J, Rico V, Cotrino J and Gonzalez-Elipe A R 2015 A. Palmero *Plasma Processes Polym.* **12** 719

[39] Mansour M, Keita A-S, Gallas B, Rivory J, Besnard A and Martin N 2010 *Opt. Mater.* **32** 1146

[40] Abadias G, Angay F, Mareus R and Mastail C 2019 *Coatings* **9** 712

[41] Choukourov A, Solar P, Polonskyi O, Hanus J, Drabik M, Kylian O, Pavlova E, Slavinska D and Biederman H 2010 *Plasma Process. Polym.* **7** 25–32

[42] Collado V, Martin N, Pedrosa P, Rauch J-Y, Horakova M, Yazdi M A P and Billard A 2016 *Surf. Coat. Technol.* **304** 476

[43] Pedrosa P, Martin N, Salut R, Yazdi M A P and Billard A 2016 *Mater. Lett.* **174** 162

[44] Le Bellac D, Azens A and Granqvist C G 1995 *Appl. Phys. Lett.* **66** 1715

[45] El Beainou R, Garcia-Valenzuela A, Raschetti M, Cote J-M, Alvarez R, Palmero A, Potin V and Martin N 2020 *Mater. Lett.* **264** 127381

[46] Muñoz-Piña S *et al* 2022 *Surf. Coat. Technol.* **436** 128293

[47] SRIM 2013 www.srim.org (last accessed on December 2023)

[48] van Aeken K 2023 available at www.draft.ugent.be (last accessed on December 2023)

[49] van Aeken K, Mahieu S and Depla D 2008 *J. Phys. D: Appl. Phys.* **41** 20530

[50] Shaginyan L R, Han J G, Shaginyan V R and Musil J 2006 *J. Vac. Sic. Technol.*A **24** 1083

[51] Shaginyan L R, Kim Y J, Han J G, Britun N V, Musil J and Belousov I V 2007 *Surf. Coat. Technol.* **202** 486

[52] Gauter S, Haase F and Kersten H 2019 *Thin Solid Films* **669** 8

[53] Gao D Z, Watkins M B and Shluger A L 2012 *J. Phys. Chem.*C **116** 1471